engineering proceedings

MDPI

Proceeding Paper

Intralaminar Fracture Calibration of Fabric Material Card for Non-Local Damage Crash Modelling †

Maria Pia Falaschetti *, Francesco Semprucci, Johan Birnie Hernández, Luca Raimondi, Enrico Troiani and Lorenzo Donati

Department of Industrial Engineering, University of Bologna, Viale Risorgimento 2, 40136 Bologna, Italy; francesco.semprucci2@unibo.it (F.S.); johan.birnie2@unibo.it (J.B.H.); luca.raimondi@unibo.it (L.R.); enrico.troiani@unibo.it (E.T.); l.donati@unibo.it (L.D.)

* Correspondence: mariapi.falaschetti2@unibo.it

† Presented at the 8th International Conference of Engineering Against Failure (ICEAF VIII), Kalamata, Greece, 22–25 June 2025.

Abstract

Crashworthiness refers to a structure's ability to absorb and dissipate impact energy through controlled deformation, thereby enhancing protection of vehicle occupants and onboard equipment. Composite materials possess significant potential in crashworthy airborne and ground vehicle structures due to their favourable specific energy absorption. However, their performance depends on several design factors such as materials, stacking sequences, and geometry. To reduce development costs and time to market, numerical simulations have become a necessary tool for optimising these factors. A challenge in this approach is the calibration of models, which is decisive for ensuring reliable and predictive simulations. Among other approaches, Non-local Damage Models have demonstrated reliability in simulating crashworthy composite structures. This work presents the intralaminar fracture energy calibration of fabric ply within a Waas–Pineda model, as implemented in ESI Virtual Performance Solutions, using Compact Tension and Compact Compression tests.

Keywords: intralaminar fracture toughness; Waas–Pineda model; fabric composite

check for updates

Academic Editors: Spiros Pantelakis and Spyros Diplas

Published: 15 December 2025

Citation: Falaschetti, M.P.; Semprucci, F.; Birnie Hernández, J.; Raimondi, L.; Troiani, E.; Donati, L. Intralaminar Fracture Calibration of Fabric Material Card for Non-Local Damage Crash Modelling. *Eng. Proc.* **2025**, *119*, 19. https://doi.org/10.3390/engproc2025119019

Copyright: © 2025 by the authors. Licensee MDPI, Basel, Switzerland. This article is an open access article distributed under the terms and conditions of the Creative Commons Attribution (CC BY) license (https://creativecommons.org/licenses/by/4.0/).

1. Introduction

Crash-absorbing structures guarantee the safety of their occupants and payload in both aeronautical and automotive vehicles [1,2]. Composite materials are generally used in energy-absorbing structures due to their high performance [3,4]. However, crashworthiness properties are affected by several design factors such as material constituents [5–8], trigger [9], profile geometry [10], working environment [11,12], etc. Experimental studies assessing the effects of each parameter would lead to costly and time-consuming processes. Therefore, different numerical models have been developed to reproduce crushing events. Large structures are usually modelled with simplified approaches, losing predictive capabilities but allowing rapid evaluation of multiple structures. More detailed simulations allow for an in-depth analysis of crushing physics but require higher computational times and longer preprocessing phases. The choice of damage models is influenced by the aim of the numerical analysis: different models perform better under different conditions and requirements. Progressive Failure Models (PFM [13,14]) are usually implemented in large-scale simulations, with no chance to analyse crushing morphology. Continuum Damage Models (CDM [15,16]) use damage parameters to assess material damage evolution and material

degradation throughout the crushing event. Non-local Damage Models (NDM [17,18]) have the flexibility of these previous models whilst overcoming the feature mesh sensitivity of CDMs. The latter is widely used for crashworthiness simulations, but it requires the measurement of several material constitutive parameters [9,19].

This manuscript focuses on the calibration of an NDM (Waas–Pineda [20,21]) through Compact Tension (CT) and Compact Compression (CC) tests on fabric composite laminates for ESI-VPS Visual-Crash PAM software.

2. Materials and Methods

2.1. Numerical Model

In a compressive crash event of composite structures, different failure modes can be identified. For the lamina, the most important are fibre fragmentation, splaying of fronds, and wall buckling; each is associated with different energy dissipations [10,22], whilst, due to the layered nature of a composite component, the most important failure between laminae is delamination. Numerical simulations, therefore, should implement these failure modes correctly to ensure reliable results. A common way to model a composite laminate is with shell layers, representing the different plies, and ties between them to simulate interlaminar interactions.

The following sections provide a brief description of the ESI-VPS shell modelling related to fabric composite plies.

2.1.1. Basic Shell Model

The stiffness tensor for a fabric composite lamina modelled with shells can be defined as follows:

$$\begin{bmatrix} \varepsilon_{11} \\ \varepsilon_{22} \\ \gamma_{12} \end{bmatrix} = \begin{bmatrix} \frac{1}{E_{11}^{d}} & -\frac{v_{12}}{E_{11}^{0}} & 0 \\ -\frac{v_{12}}{E_{11}^{0}} & \frac{1}{E_{22}^{d}} & 0 \\ 0 & 0 & \frac{1}{E_{12}^{d}} \end{bmatrix} \begin{bmatrix} \sigma_{11} \\ \sigma_{22} \\ \tau_{12} \end{bmatrix} \quad (1)$$

where $E_{ij}^{d} = (1 - d_{ij}) E_{ij}^{0}$ represents the damage modelled through the degradation of material stiffness and d_{ij} is the numerical damage parameter, varying from 0 (as-built conditions) to 1 (ultimate failure). The superscripts 0 and d refer to the undamaged and damaged quantities. The subscripts ij refer to the property direction: 11 and 22 for the fibre directions, and 12 for the shear direction.

2.1.2. Waas–Pineda Model (WP)

The WP model [20,21,23] implemented in the software adds the formulation of a non-local crack to the orthotropic elasticity and matrix plasticity implemented in the generic orthotropic material card [6,23–25]. This leads to effective material softening during the damaging state.

In the WP model, there are three distinct material states: the continuum, cohesive, and post-damage states, with irreversible transitions between them (Figure 1). The transition from the continuum state to the cohesive state (where the damage propagates) is activated by a quadratic failure criterion (stress-based or strain-based), whilst the transition from the cohesive to post-damage state relies on a maximum admissible damage criterion.

The cohesive state uses bilinear cohesive traction separation laws and is determined by the cohesive stiffness $K = \frac{\sigma}{\delta}$ and the damage parameters. The model describes the effects of five failure modes: fibre rupture under tension, matrix cracking and fibre–matrix debonding under tension, fibre kinking under compression, matrix cracking under transverse compression, and matrix shear cracking. The post-damage state is defined by a prescribed critical

$D_{max} = \left(1 - \sigma_{ij}/\sigma_{ij}^{0}\right)$, which is unique for all damage modes. The element elimination is set up on the equivalent shear strain limit $\varepsilon_{elim} = \varepsilon_{ij} - (1/3)\varepsilon_{kk}\delta_{ij}$.

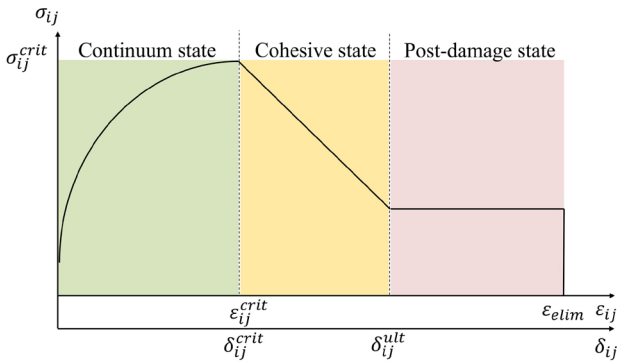

Figure 1. Waas–Pineda damage model: material states.

2.1.3. Delamination

The interlaminar interaction in ESI-VPS can be modelled as 1D beams connecting nodes belonging to two adjacent surfaces. Main interlaminar properties derive from standard Mode I and Mode II experimental tests, whilst the mixed-mode interaction can be implemented using either the Benzeggagh–Kenane fracture criterion [26] or power law models [23].

2.2. Experimental Set Up and Tests

A fabric laminate $[(90/0)_f]_{4s}$ was manufactured using a plain weave carbon/epoxy prepreg (GG285P-DT120, Delta Tech S.p.A., Lucca, Italy). The cured thickness of the material was 3.2 mm.

In the literature, several test methods to measure the intralaminar fracture energy have been proposed, and the most valuable ones are the CT and the CC tests [27–31]. Both kinds of coupons were obtained by a milling process using a CNC machine. To introduce the sharp crack required for the CT specimens, a diamond-coated disc saw was used to create an initial notch up to 20 mm in length. This was followed by an additional 10 mm extension using a 1 mm thick disc saw and subsequently a razor blade. Both CT and CC tests were conducted on a universal testing machine equipped with a 10 kN load cell, operating under displacement control at a rate of 1 mm/min.

To assess the crashworthiness characteristics, this study employs self-supported coupons, which consist of semicircular corrugated specimens, as described in the authors' previous works [7,8]. The test consisted of a quasi-static compression between two plates with a 2 mm/min displacement rate.

2.3. Model Calibration and Procedure Validation

The calibration procedure for the WP model is structured as follows:

1. From experimental tests, the ultimate failure stresses σ^{crit} are obtained.
2. The ultimate tensile, compressive, and shear stresses are used in the material card as stress thresholds for damage initiation.
3. From the CT and CC tests, the fibre fracture energies (EFRt for the tensile and EFRc for the compressive energies) are calculated and applied to the model.
4. Simulations are performed to assess the energies' values with respect to the mesh dimensions and, consequently, to tune D_{max} and ε_{lim} with the aim of fulfilling the numerical stability.

The fourth point of the calibration procedure takes place by means of CT and CC numerical simulations.

In this paper, three different mesh dimensions (0.25 mm, 0.5 mm, and 1 mm) are considered. Independent of the different mesh dimensions, the CC and CT specimens are modelled with identical settings: out-of-plane displacement is restricted, limiting the buckling instability; the specimens are loaded by means of a constant displacement applied on the areas mimicking the experimental pinholes.

For the calibration validation, a numerical-experimental comparison is needed. Therefore, a numerical simulation of the crashworthiness tests is implemented. The model consists of six shells, interleaved by five cohesive layers. One end of the specimen is fixed, whilst the opposite end is modelled with a chamfer geometry to represent the experimental conditions. The striker wall is modelled as a rigid body, and the test is performed under displacement control. All three mesh dimensions are simulated and compared with the experimental outcomes.

3. Results and Discussion

3.1. Experimental Results

Data postprocessing for the tensile, compressive, and in-plane shear tests is carried out following the guidelines described in ASTM D3039 [32], ASTM D3410 [33], and ASTM D3518 [34], respectively.

For the fracture toughness, data analysis is conducted according to the ASTM E399 [35] modified orthotropy method and the Compliance Calibration [36] method for the CT and CC tests, respectively. The measured energies are listed in Table 1.

Table 1. Waas–Pineda damage model: fracture toughness parameters.

Property	Value
Axial tensile fracture energy	105 J/m^2
Axial compressive fracture energy	85 J/m^2
Transverse tensile fracture energy	105 J/m^2
Transverse compressive fracture energy	85 J/m^2
Shear fracture energy	38 J/m^2

3.2. Numerical Calibration

As previously discussed, the WP model needs to be calibrated: the intralaminar fracture energies and numerical parameters have to be tuned according to mesh dimension and numerical stability. The first stage is to verify if the experimentally measured values are suitable for the model's mesh size.

The experimentally determined energies are used in the CT and CC simulations, whilst values of 0.85 for D_{max} and 0.15 for ε_{lim} are chosen [6,19] for the three selected mesh sizes.

Figure 2 illustrates how the 0.25 mm mesh dimension with the base material characteristics captures experimental behaviour with already good agreement, solely necessitating a calibration of its numerical parameters (D_{max} and ε_{lim}). In contrast, the 1 mm mesh shows a weak correlation, highlighting the model's dependence on intralaminar fibre fracture energy. Figure 3 displays the results of the calibration for the 1 mm mesh. The intralaminar fibre energies of 55 J/m^2 and 65 J/m^2 for the tensile and compressive loading conditions, respectively, shows an optimum behaviour and are selected as tuned energy values. At the same time, the optimised values for this mesh dimension for D_{max} and ε_{lim} are 0.85 and 0.3, respectively.

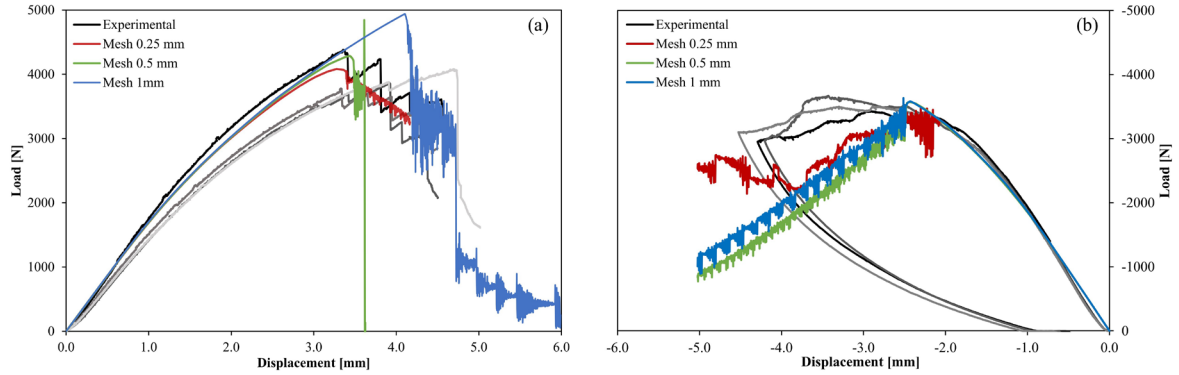

Figure 2. Numerical results for CT (**a**) and CC (**b**) simulations implementing experimentally measured material characteristics. The 0.25 mm, 0.5 mm and 1 mm mesh dimensions are compared with experimental curves.

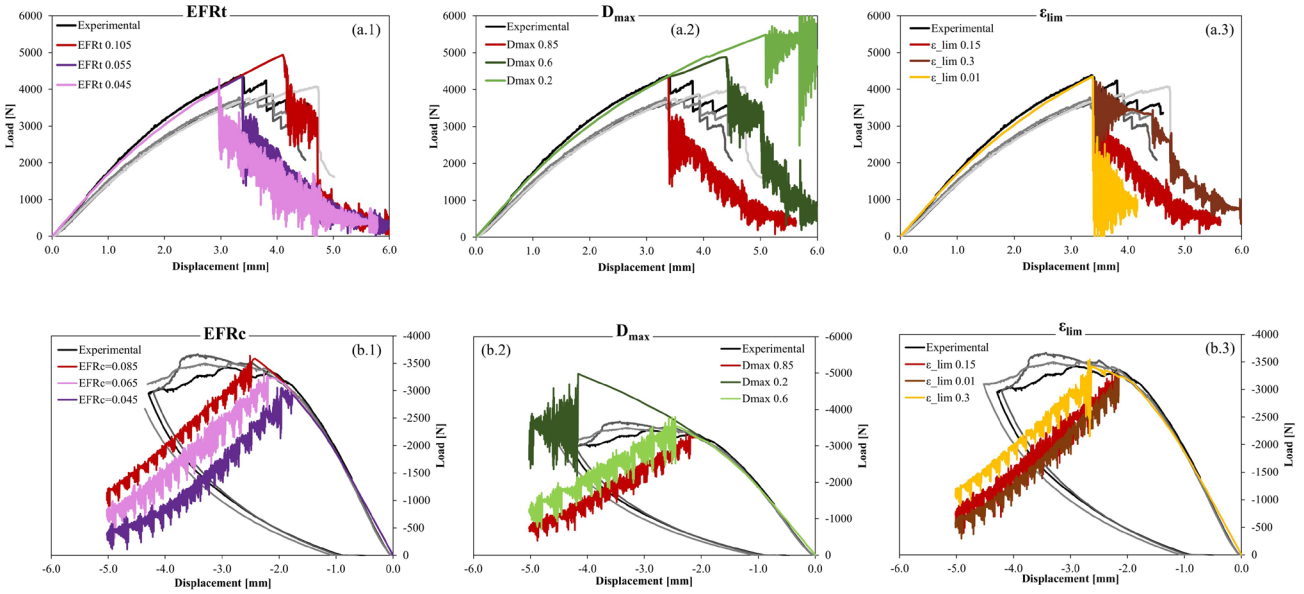

Figure 3. The 1 mm mesh CT (**a.1–a.3**) and CC (**b.1–b.3**) calibration results (different values of EFRt, EFRc, D_{max}, and ε_{lim}).

3.3. Crashworthiness Experimental–Numerical Comparison

The material card, calibrated by means of the CT and CC simulations, has to be validated through crash simulations.

Results from two models with mesh sizes of 0.5 and 1 mm are shown in Figure 4.

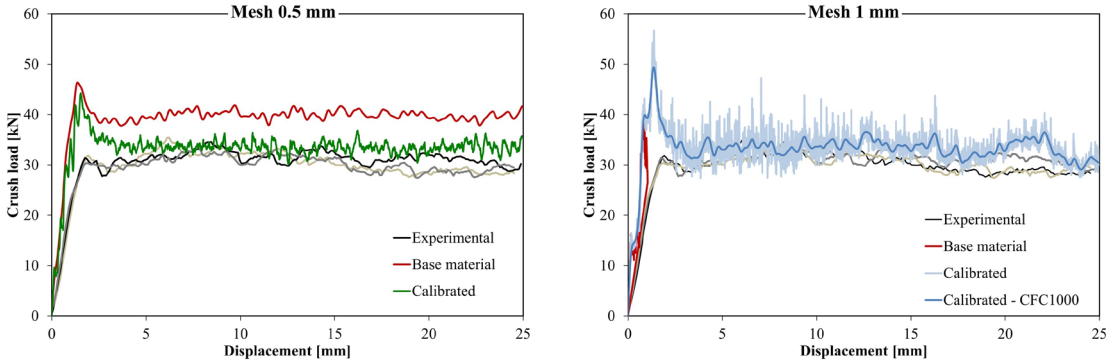

Figure 4. Crashworthiness experimental and simulation results: 0.5 mm and 1 mm mesh comparison.

Both models demonstrate good agreement with the experimental outcomes only when the calibrated material card is used. In the case of the 0.5 mm mesh model, the base material card results in an overestimation of the load-bearing capability of the specimen. For the 1 mm mesh, on the other hand, the base card implementation corresponds to numerical instability and fails to converge before the failure of the trigger. After implementing the calibrated material card, both the 0.5 mm and the 1 mm mesh models shows good agreement with the experimental curves. The 1 mm model presents higher noise in the load–displacement results due to the oscillation generated by the failure and elimination of the larger elements. However, the filtered results shows a behaviour that could be easily superimposed on the experimental ones. The only incongruity lies in the initial stage, where the numerical trigger geometry does not accurately capture the experimental behaviour, requiring specific optimisation. Both mesh dimensions can be effectively utilised for crashworthiness simulations. However, the computational effort required may influence the choice of which model to use. The 0.5 mm mesh model takes 207 hours of CPU time, compared to just 64 hours for the alternative model.

4. Conclusions

This study presented the calibration of intralaminar fracture toughness for the Waas–Pineda NDM using Compact Compression (CC) and Compact Tension (CT) tests. The calibration process involved a series of CT and CC simulations aimed at evaluating the influence of mesh size on the computed intralaminar fracture energy, as well as on the critical values of maximum damage and equivalent shear strain. The calibrated parameters, incorporated into the material cards, were subsequently validated through crashworthiness tests performed on self-supporting specimens. The numerical results from these crash simulations showed good agreement with experimental data, thereby confirming the accuracy and robustness of the proposed calibration procedure.

Author Contributions: Conceptualization, M.P.F. and L.R.; Methodology, M.P.F., F.S., J.B.H. and L.R.; Software, M.P.F.; Validation, M.P.F.; Formal Analysis, M.P.F.; Investigation, M.P.F.; Data Curation, M.P.F.; Writing—Original Draft Preparation, M.P.F.; Writing—Review and Editing, M.P.F., F.S., J.B.H., and E.T.; Visualisation, F.S. and J.B.H.; Supervision, E.T.; Funding Acquisition, E.T. and L.D.; Project Administration, L.D. All authors have read and agreed to the published version of the manuscript.

Funding: M.P.F. acknowledges MOST-Sustainable Mobility National Research Center, which is funded by the European Union NextGenerationEU (Piano Nazionale di Ripresa e Resilienza (PNRR)—Missione 4 Componente 2, Investimento 1.4—D.D. 1033 17/06/2022, CN00000023, CUP: J33C22001120001). F.S. acknowledges the support of the SMALSAT 'Solar Panel Design for the SMAL-SAT nanosatellite' project, funded under PR FESR EMILIA ROMAGNA 2021-2027 CUP: J47G22000720003. J.B.H. acknowledges the support of the European Union NextGenerationEU through the Italian Ministry of University and Research under PNRR, Mission 4 Component 1, Investment 4.1 and 3.4; CUP: J33C23002650002. L.R. and L.D. acknowledge the support of the Ecosystem for Sustainable Transition in Emilia-Romagna Project, funded under the National Recovery and Resilience Plan (NRRP), Mission 04 Component 2 Investment 1.5—NextGenerationEU, call for tender n. 3277 dated 30 December 2021, Award Number: 0001052 dated 23 June 2022, CUP: B33D21019790006.

Institutional Review Board Statement: Not applicable.

Informed Consent Statement: Not applicable.

Data Availability Statement: The datasets presented in this article are not readily available because the data are part of an ongoing study.

Conflicts of Interest: The authors declare no conflicts of interest. The funders had no role in the design of the study; in the collection, analyses, or interpretation of data; in the writing of the manuscript; or in the decision to publish the results.

Abbreviations

The following abbreviations are used in this manuscript:

CC	Compact Compression
CDM	Continuum Damage Model
CT	Compact Tension
ESI-VPS	ESI Virtual Performance Solution
NDM	Non-local Damage Model
PFM	Progressive Damage Model
WP	Waas–Pineda

References

1. Lopresto, V. Crashworthiness Design and Evaluation of Civil Aircraft Structures. *Prog. Aerosp. Sci.* **2024**, *148*, 101000. [CrossRef]
2. Bisagni, C.; Di Pietro, G.; Fraschini, L.; Terletti, D. Progressive Crushing of Fiber-Reinforced Composite Structural Components of a Formula One Racing Car. *Compos. Struct.* **2005**, *68*, 491–503. [CrossRef]
3. Thornton, P.H. Energy Absorption in Composite Structures. *J. Compos. Mater.* **1979**, *13*, 247–262. [CrossRef]
4. Raimondi, L.; Bernardi, F. Advanced Hybrid Laminates: Elastomer Integration for Optimized Mechanical Properties. *Int. J. Adv. Manuf. Technol.* **2025**, *136*, 3177–3195. [CrossRef]
5. Ramakrishna, S. Microstructural Design of Composite Materials for Crashworthy Structural Applications. *Mater. Des.* **1997**, *18*, 167–173. [CrossRef]
6. Rondina, F.; Falaschetti, M.P.; Zavatta, N.; Donati, L. Numerical Simulation of the Compression Crushing Energy of Carbon Fiber-Epoxy Woven Composite Structures. *Compos. Struct.* **2023**, *303*, 116300. [CrossRef]
7. Falaschetti, M.P.; Rondina, F.; Maccaferri, E.; Mazzocchetti, L.; Donati, L.; Zucchelli, A.; Giorgini, L. Improving the Crashworthiness of CFRP Structures by Rubbery Nanofibrous Interlayers. *Compos. Struct.* **2023**, *311*, 116845. [CrossRef]
8. Falaschetti, M.P.; Semprucci, F.; Raimondi, L.; Serradimigni, D. Experimental and Numerical Assessment of Sheet Molding Compound Composite Crushing Behavior. *J. Mater. Eng. Perform.* **2025**, *34*, 15281–15292. [CrossRef]
9. Falaschetti, M.P.; Semprucci, F.; Birnie Hernández, J.; Troiani, E. Experimental and Numerical Assessment of Crashworthiness Properties of Composite Materials: A Review. *Aerospace* **2025**, *12*, 122. [CrossRef]
10. Mamalis, A.G.; Manolakos, D.E.; Ioannidis, M.B.; Papapostolou, D.P. On the Experimental Investigation of Crash Energy Absorption in Laminate Splaying Collapse Mode of FRP Tubular Components. *Compos. Struct.* **2005**, *70*, 413–429. [CrossRef]
11. Falaschetti, M.P.; Scafé, M.; Zavatta, N.; Troiani, E. Hygrothermal Ageing Influence on BVI-Damaged Carbon/Epoxy Coupons under Compression Load. *Polymers* **2021**, *13*, 2038. [CrossRef] [PubMed]
12. Sebaey, T.A. Effect of Exposure Temperature on the Crashworthiness of Carbon/Epoxy Composite Rectangular Tubes Under Quasi-Static Compression. *Polymers* **2020**, *12*, 2028. [CrossRef] [PubMed]
13. Chang, F.K.; Chang, K.Y. A Progressive Damage Model for Laminated Composites Containing Stress Concentrations. *J. Compos. Mater.* **2016**, *21*, 834–855. [CrossRef]
14. Feraboli, P.; Wade, B.; Deleo, F.; Rassaian, M.; Higgins, M.; Byar, A. LS-DYNA MAT54 Modeling of the Axial Crushing of a Composite Tape Sinusoidal Specimen. *Compos. Part A Appl. Sci. Manuf.* **2011**, *42*, 1809–1825. [CrossRef]
15. Johnson, A.F.; Pickett, A.K.; Rozycki, P. Computational Methods for Predicting Impact Damage in Composite Structures. *Compos. Sci. Technol.* **2001**, *61*, 2183–2192. [CrossRef]
16. Sokolinsky, V.S.; Indermuehle, K.C.; Hurtado, J.A. Numerical Simulation of the Crushing Process of a Corrugated Composite Plate. *Compos. Part A Appl. Sci. Manuf.* **2011**, *42*, 1119–1126. [CrossRef]
17. Germain, N.; Besson, J.; Feyel, F. Composite Layered Materials: Anisotropic Nonlocal Damage Models. *Comput. Methods Appl. Mech. Eng.* **2007**, *196*, 4272–4282. [CrossRef]
18. Zobeiry, N.; Forghani, A.; McGregor, C.; McClennan, S.; Vaziri, R.; Poursartip, A. Effective Calibration and Validation of a Nonlocal Continuum Damage Model for Laminated Composites. *Compos. Struct.* **2017**, *173*, 188–195. [CrossRef]
19. Falaschetti, M.P.; Rondina, F.; Zavatta, N.; Troiani, E.; Donati, L. Effective Implementation of Numerical Models for the Crashworthiness of Composite Laminates. *Eng. Fail. Anal.* **2024**, *160*, 108196. [CrossRef]
20. Pineda, E. A Novel Multiscale Physics-Based Progressive Damage and Failure Modeling Tool for Advanced Composite Structures. Ph.D. Thesis, University of Michigan, Ann Arbor, MI, USA, 2012.
21. Pineda, E.J.; Waas, A.M. Numerical Implementation of a Multiple-ISV Thermodynamically-Based Work Potential Theory for Modeling Progressive Damage and Failure in Fiber-Reinforced Laminates. *Int. J. Fract.* **2013**, *182*, 93–122. [CrossRef]
22. Mamalis, A.G.; Manolakos, D.E.; Ioannidis, M.B.; Papapostolou, D.P. Crashworthy Characteristics of Axially Statically Compressed Thin-Walled Square CFRP Composite Tubes: Experimental. *Compos. Struct.* **2004**, *63*, 347–360. [CrossRef]

23. ESI-Software. *Virtual Performance Solution Solver Reference Manual*, 2023rd ed.; ESI: Bagneux, France, 2023.
24. Ladevèze, P. A Damage Computational Method for Composite Structures. *Comput. Struct.* **1992**, *44*, 79–87. [CrossRef]
25. Ladevèze, P.; Allix, O.; Gornet, L.; Lévêque, D.; Perret, L. A Computational Damage Mechanics Approach for Laminates: Identification and Comparison with Experimental Results. *Stud. Appl. Mech.* **1998**, *46*, 481–500. [CrossRef]
26. Benzeggagh, M.L.; Kenane, M. Measurement of Mixed-Mode Delamination Fracture Toughness of Unidirectional Glass/Epoxy Composites with Mixed-Mode Bending Apparatus. *Compos. Sci. Technol.* **1996**, *56*, 439–449. [CrossRef]
27. Laffan, M.J.; Pinho, S.T.; Robinson, P.; Iannucci, L. Measurement of the in Situ Ply Fracture Toughness Associated with Mode I Fibre Tensile Failure in FRP. Part I: Data Reduction. *Compos. Sci. Technol.* **2010**, *70*, 606–613. [CrossRef]
28. Pinho, S.T.; Robinson, P.; Iannucci, L. Fracture Toughness of the Tensile and Compressive Fibre Failure Modes in Laminated Composites. *Compos. Sci. Technol.* **2006**, *66*, 2069–2079. [CrossRef]
29. Blanco, N.; Trias, D.; Pinho, S.T.; Robinson, P. Intralaminar Fracture Toughness Characterisation of Woven Composite Laminates. Part II: Experimental Characterisation. *Eng. Fract. Mech.* **2014**, *131*, 361–370. [CrossRef]
30. Swolfs, Y.; Geboes, Y.; Gorbatikh, L.; Pinho, S.T. The Importance of Translaminar Fracture Toughness for the Penetration Impact Behaviour of Woven Carbon/Glass Hybrid Composites. *Compos. Part A Appl. Sci. Manuf.* **2017**, *103*, 1–8. [CrossRef]
31. Reiner, J.; Vaziri, R.; Zobeiry, N. Machine Learning Assisted Characterisation and Simulation of Compressive Damage in Composite Laminates. *Compos. Struct.* **2021**, *273*, 114290. [CrossRef]
32. *ASTM D3039/D3039M-08*; Standard Test Method for Tensile Properties of Polymer Matrix Composite Materials. ASTM: West Conshohocken, PA, USA, 2008.
33. *ASTM D3410/D3410M*; Standard Test Method for Compressive Properties of Polymer Matrix Composite Materials with Unsupported Gage Section by Shear Loading. ASTM: West Conshohocken, PA, USA, 1997.
34. *ASTM D3518*; In-Plane Shear Response of Polymer Matrix Composite Materials by Tensile Test of ±45 Deg Laminate. ASTM: West Conshohocken, PA, USA, 2013.
35. *ASTM E399*; Standard Test Method for Linear-Elastic Plane-Strain Fracture Toughness of Metallic Materials. ASTM: West Conshohocken, PA, USA, 1997.
36. Liu, H.; Falzon, B.G.; Catalanotti, G.; Tan, W. An Experimental Method to Determine the Intralaminar Fracture Toughness of High-Strength Carbon-Fibre Reinforced Composite Aerostructures. *Aeronaut. J.* **2018**, *122*, 1352–1370. [CrossRef]

Disclaimer/Publisher's Note: The statements, opinions and data contained in all publications are solely those of the individual author(s) and contributor(s) and not of MDPI and/or the editor(s). MDPI and/or the editor(s) disclaim responsibility for any injury to people or property resulting from any ideas, methods, instructions or products referred to in the content.